Excited states and signature inversion in ^{116}Cs

J. F. Smith,[1,*] C. J. Chiara,[2,3] M. P. Carpenter,[4] C. N. Davids,[4] M. Devlin,[3,5] D. B. Fossan,[2] S. J. Freeman,[1] R. V. F. Janssens,[4] D. R. LaFosse,[2] D. G. Sarantites,[3] D. Seweryniak,[4] K. Starosta,[6] R. Wadsworth,[7] A. N. Wilson,[7,†] and R. Wyss[8]

[1]*Schuster Laboratory, University of Manchester, Manchester, M13 9PL, United Kingdom*

[2]*Department of Physics and Astronomy, State University of New York at Stony Brook, Stony Brook, New York 11794, USA*

[3]*Department of Chemistry, Washington University, St. Louis, Missouri 63130, USA*

[4]*Argonne National Laboratory, Argonne, Illinois 60439, USA*

[5]*LANSCE-3, Los Alamos National Laboratory, Los Alamos, New Mexico 87545, USA*

[6]*National Superconducting Cyclotron Laboratory and Department of Physics and Astronomy, Michigan State University, East Lansing, Michigan 48854, USA*

[7]*Department of Physics, University of York, Heslington, York, YO10 5DD, United Kingdom*

[8]*Royal Institute of Technology, Physics Department Frescati, Frescativägen 24, S-104 05 Stockholm, Sweden*

(Received 16 September 2005; published 12 September 2006)

Excited states have been observed for the first time in the very neutron-deficient, odd-odd nucleus, $^{116}_{55}Cs_{61}$. The assignment to ^{116}Cs has been made by the detection of γ rays in coincidence with evaporated charged particles and with evaporation residues. The observed states form a rotational band which has been assigned to the $\nu(h_{11/2}) \otimes \pi(h_{11/2})$ configuration. Tentative spin assignments have been made on the basis of systematic comparisons with neighboring cesium isotopes. A low-spin signature inversion is observed in the band at a rotational frequency of about 0.23 MeV/$\hbar$. The observed signature inversions in the odd-odd $^{116-126}$Cs isotopes have been compared with the results of extended total Routhian surface calculations, in which signature inversion arises as a consequence of quadrupole-pairing correlations and triaxial deformation. As previously shown for some of the odd-odd $A \simeq 120$ isotopes, the calculations reproduce the signature inversions reasonably well.

DOI: 10.1103/PhysRevC.74.034310 PACS number(s): 21.10.Re, 23.20.Lv, 27.60.+j, 29.30.Kv

I. INTRODUCTION

Over the past 20 years, signature inversion [1–4] has become a well-established phenomenon in two-quasiparticle rotational bands in odd-odd nuclei. Signature inversion describes the situation in which states that should lie lowest in energy, according to the rotational model, are displaced upward below a critical *inversion frequency*. Despite the observation of signature inversion in many different nuclei, and despite numerous theoretical interpretations, a satisfactory explanation of the phenomenon has yet to be found. Indeed, it is still not clear whether a universal description exists, or if different mechanisms are responsible for the phenomenon in different mass regions.

Signature [5] is a symmetry that results from an invariance of the cranking Hamiltonian with respect to a rotation by 180° about an axis perpendicular to the nuclear symmetry axis. If the eigenvalue of the operator which reverses the direction of the symmetry axis is denoted by r, then in the principal-axis cranking (PAC) description of nuclear rotation, the *signature quantum number* α is defined by the relation $r = e^{-i\pi\alpha}$. Rotational bands are often characterized by α, which defines the spin (I) sequence within the band according to $I = \alpha + 2n$, where $n = 0, 1, 2, \ldots$. Two-quasiparticle bands in odd-odd nuclei are formed of two $\Delta I = 2$ sequences, each with a different value of α. In the rotational model, one of the sequences is usually expected to lie lower in excitation energy, and is said to have *favored* signature α_f; while the other sequence has *unfavored* signature α_u. For such bands, the favored signature α_f is expected to be $\alpha_f = (1/2)|(-1)^{(j_n-1/2)} + (-1)^{(j_p-1/2)}|$ where j_n and j_p are the spins of the valence neutron and proton, respectively, and $\alpha_u = |1 - \alpha_f|$ [6].

The energy difference between the two sequences is directly related to the energy difference between the quasiparticle Routhians [7], known as the *signature splitting*. The size of this quantity is dependent on several factors such as the characteristics of the single-particle orbitals occupied by the valence nucleons, and the shape of the nucleus. Typically, signature splitting increases with rotational frequency ω, due to an increase in the Coriolis force. However, in some two-quasiparticle bands in odd-odd nuclei, the splitting has been observed to *decrease* with rotational frequency, and even to change sign [2–4]. In these bands, the states associated with the unfavored signature lie lower in energy at the lowest rotational frequencies. This phenomenon is known as *signature inversion*, and the rotational frequency at which the signature splitting changes sign is known as the *inversion frequency*.

Signature inversion has mainly been observed in three regions of nuclei, with masses $A \simeq 160$ [2], $A \simeq 120$ [3,4,8], and $A \simeq 70$ [9,10]. In the $A \simeq 120$ nuclei, signature inversion occurs in the $\nu(h_{11/2}) \otimes \pi(h_{11/2})$ bands of odd-odd $_{53}$I, $_{55}$Cs, $_{57}$La, $_{59}$Pr, $_{61}$Pm, and $_{63}$Eu isotopes ([3,4,8] and references therein). In the cesium isotopes, the proton Fermi level lies at or near the prolate-driving $\Omega = 1/2h_{11/2}$ orbital. For the heavier ($A \gtrsim 124$) isotopes, the neutron Fermi level lies in the oblate-driving mid- to high-Ω $h_{11/2}$ orbitals. The competing

*Electronic address: John.F.Smith@Manchester.ac.uk

†Present address: Department of Nuclear Physics, RSPhysSE, Australian National University, Canberra ACT 0200, Australia.

neutron and proton shape-driving properties can lead to a variety of nuclear shapes, including triaxial deformations. In the lighter ($A \lesssim 120$) isotopes, the neutron Fermi level lies in the low-Ω $h_{11/2}$ orbitals, which can lead a large overlap of the neutron and proton wave functions, and consequently a large neutron-proton (np) interaction. Both triaxial deformation and np interactions have been proposed as the mechanisms responsible for causing signature inversion.

Prior to the present work, signature-inversion frequencies had been identified in the $\nu(h_{11/2}) \otimes \pi(h_{11/2})$ bands of the $Z = 55$ $^{118-126}$Cs isotopes [11–18]; the most neutron-deficient odd-odd cesium isotope in which excited states had been observed was $^{118}Cs_{63}$ [12]. It is expected that the np interaction will increase in significance when approaching $N = Z$, so it is important that the more neutron-deficient isotopes be studied, in order to set apart the different theoretical interpretations. Experimental investigations of the cesium isotopes become increasingly challenging for $A < 118$. The most effective way to populate high-spin states in these nuclei is to use fusion-evaporation reactions, but because the compound nuclei themselves are very neutron deficient, the evaporation of both α particles and protons is favored, and cross sections for the production of the most neutron-deficient nuclei are rather small. Such experiments are only possible with highly efficient detectors using sensitive channel-selection methods. Using such methods, the present work reports the first observation of excited states in the very neutron-deficient isotope, $^{116}_{55}Cs_{61}$.

II. EXPERIMENTAL DETAILS

In this work, excited states in ^{116}Cs were populated using the ^{58}Ni(^{64}Zn,αpn) reaction. A 265-MeV ^{64}Zn beam, provided by the Argonne Tandem-Linac Accelerator System (ATLAS) at Argonne National Laboratory, was incident upon a target consisting of two 500-μg/cm^2 self-supporting ^{58}Ni foils. Emitted γ rays were detected with the Gammasphere spectrometer [19], consisting of 101, 75% efficient Compton-suppressed germanium detectors. The detectors were arranged in 16 rings of constant polar angle θ with respect to the beam direction. The Microball charged-particle detector array, which consists of 95 CsI(Tl) scintillators [20], was used to detect evaporated protons and α particles. Reaction products recoiling out of the target entered the fragment mass analyzer (FMA) [21], where they were dispersed according to their mass M to charge-state q ratio, and subsequently detected by a parallel-plate gridded-anode avalanche counter (PGAC) at the focal plane. The FMA thus effectively enabled the mass of the reaction products to be determined. Data were recorded when either one of two trigger conditions was satisfied: (i) four suppressed germanium detectors firing within an 800-ns time window or (ii) three suppressed germanium detectors firing within 800 ns, in coincidence with a signal from the PGAC at the FMA focal plane. If present, particles detected by the Microball were included in the data for both trigger conditions.

III. DATA ANALYSIS: ASSIGNMENT OF EXCITED STATES

As a starting point in the offline analysis, all of the two- and three-fold γ-ray events were used to increment two- and three-dimensional histograms known as *matrices* and *cubes*, respectively. These histograms were analyzed using the RADWARE data-analysis codes [22]. Over 15 evaporation residues were produced in the experiment, the most intense being ^{118}Xe ($4p$ evaporation), ^{119}Cs ($3p$), ^{116}Xe ($\alpha 2p$), and ^{118}Cs ($3pn$), which are populated with fractions 0.33, 0.29, 0.15, and 0.09 of the data, respectively. Histograms were also created which were gated on different combinations of evaporated particles and on different M/q values. Discrimination between protons and α particles was achieved with the methods described in Ref. [20]. The Microball detection efficiencies were measured to be 80% for protons and 61% for α particles. For the FMA, the transmission efficiency was measured to be 4% for ^{118}Xe ($4p$ evaporation) and 1% for ^{116}Xe ($\alpha 2p$), and the M/q resolution was found to be approximately 1 in 400.

The measured particle-detection efficiencies suggested that the αp-gated matrix would contain the highest intensity of γ rays from the αpn evaporation residue, ^{116}Cs. Analysis of this matrix revealed coincident γ rays with energies 192, 216, 225, 243, 443, 635, and 650 keV that do not belong to any of the known nuclei populated in the reaction. These γ rays were, therefore, assigned as candidates for transitions in ^{116}Cs. The low-energy part of the spectrum in coincidence with the 192-keV γ ray in the αp-gated matrix is shown in Fig. 1(a). These candidate ^{116}Cs transitions were also found to be present in the α- and p-gated matrices, as well as in the matrix incremented when nothing was detected by the Microball. The intensities of the γ rays in these matrices were consistent with expectations for transitions in either the αpn or αp evaporation channels estimated from the measured particle-detection efficiencies. The candidate γ rays were not present in the $\alpha 2p$- or $2\alpha p$-gated matrices, indicating that they are associated with the evaporation of *exactly* one α particle and *exactly* one proton: that is, they belong to an isotope of cesium with $A \leqslant 117$. The production of the cesium isotopes with $A \leqslant 115$ would require two or more neutrons to be evaporated, and consequently the predicted cross sections [23] for these reaction channels are lower than would be observed in the present experiment. (For example, the cross section for $\alpha p2n$ evaporation, leading to ^{115}Cs, is less than 1 μb.) This analysis therefore suggested that the γ rays belonged to either ^{116}Cs or ^{117}Cs; therefore, the matrices gated on $A = 116$ and $A = 117$ were analyzed. The γ rays were found to be present in the $A = 116$-gated matrix, but not in the $A = 117$-gated matrix. The low-energy parts of the spectra gated on the 192-keV γ ray in the $A = 116$- and $A = 117$-gated matrices are shown in Figs. 1(b) and 1(c). Also shown in Fig. 1 are spectra gated on the 192-keV γ ray in matrices gated on both evaporated particles and mass: panel (d) is the spectrum from the matrix gated on αp and $A = 116$ and panel (e) is the spectrum from that gated on αp and $A = 117$. The candidate γ rays are clearly present on panels (b) and (d) which are gated on $A = 116$, thus allowing their unambiguous assignment to ^{116}Cs.

Using this analysis, a second set of weak, coincident γ rays, with energies 156, 201, 236, 270, 301, and 329 keV, has been tentatively assigned to ^{116}Cs. These γ rays are presumed to correspond to weak $\Delta I = 1$ transitions in a strongly coupled band. Having very low intensity, these γ rays could not be

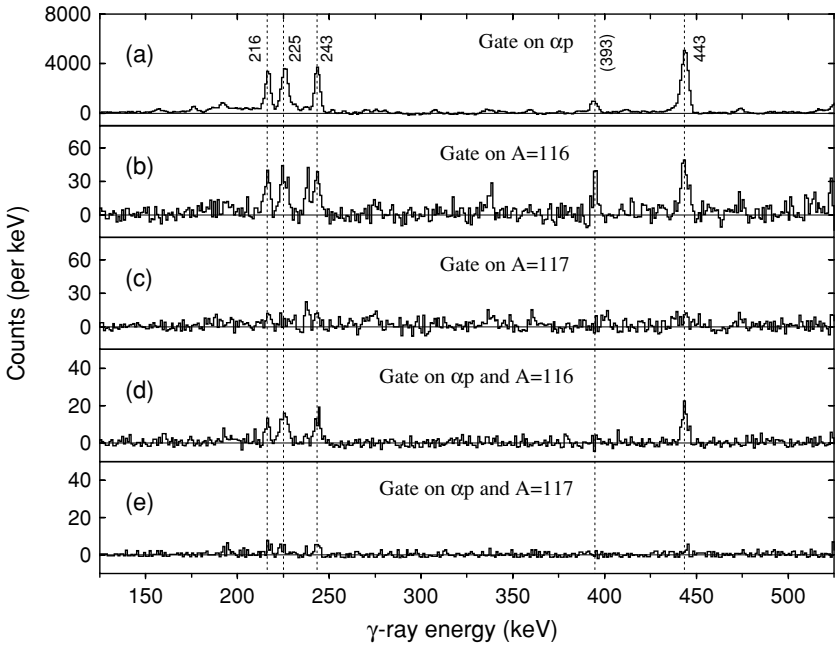

FIG. 1. Spectra demonstrating the assignment of γ rays to ^{116}Cs. All spectra are gated on the 192-keV γ ray and projected from matrices gated on charged particles and M/q (or effectively, A) as indicated on the panels. The 216-, 225-, 243-, and 443-keV transitions have been assigned to ^{116}Cs. The 393-keV γ ray is the $2^+ \rightarrow 0^+$ transition of ^{116}Xe ($\alpha 2p$ leak-through).

definitely assigned to ^{116}Cs, and are not discussed further here.

With the assignment of γ rays to ^{116}Cs made, it was then possible to relax the gating conditions to obtain the best possible spectra. To this end, a cube gated on $\alpha p, \alpha$, or p was created. Some representative spectra from this "particle-gated" cube are shown in Figs. 2 and 3: Fig. 2 shows transitions up to the highest energies observed and Fig. 3 illustrates some coincidence relationships associated with the low-energy transitions. These spectra are discussed

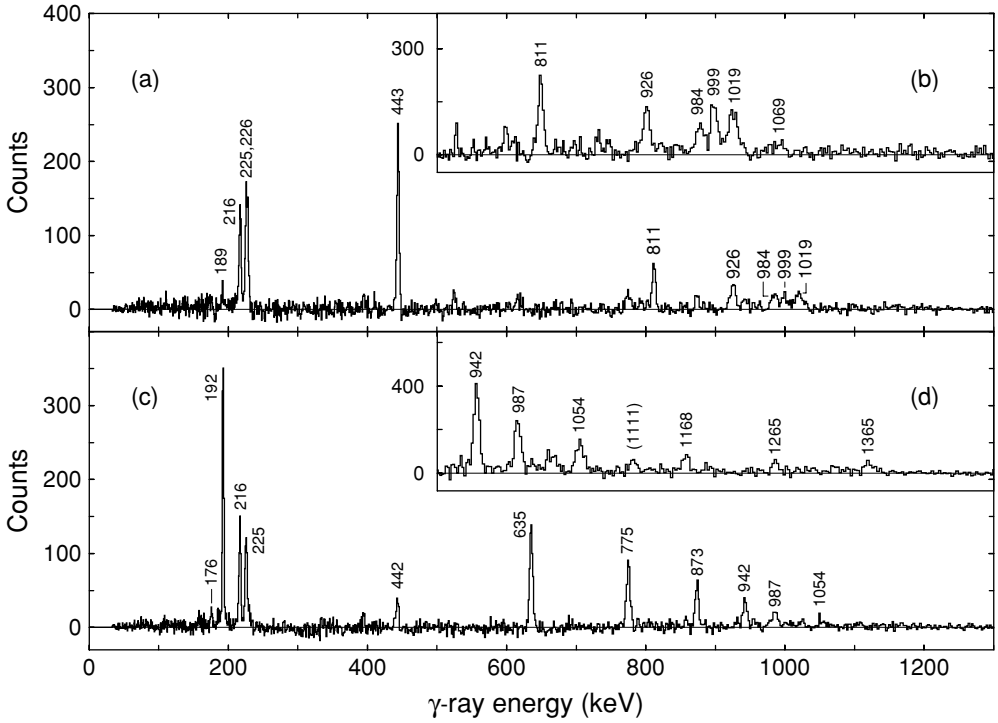

FIG. 2. Examples of γ-ray coincidence spectra, projected from the particle-gated cube, showing transitions in ^{116}Cs. Panels (a) and (b) give transitions in the even-spin ($\alpha = 0$) signature partner; (c) and (d) give transitions in the odd-spin ($\alpha = 1$) partner. Spectra were generated with the following double gates, where the numbers represent energies in keV: (a) 192 and 650; (b) (192, 216, 225, or 443) and (650, 811, or 926); (c) 243 and 443; and (d) (192, 216, 225, 243, or 443) and (635, 775, 873, 942, or 987). The 1111-keV transition in parentheses appears to be in coincidence with the ^{116}Cs transitions but could not be placed in the level scheme.

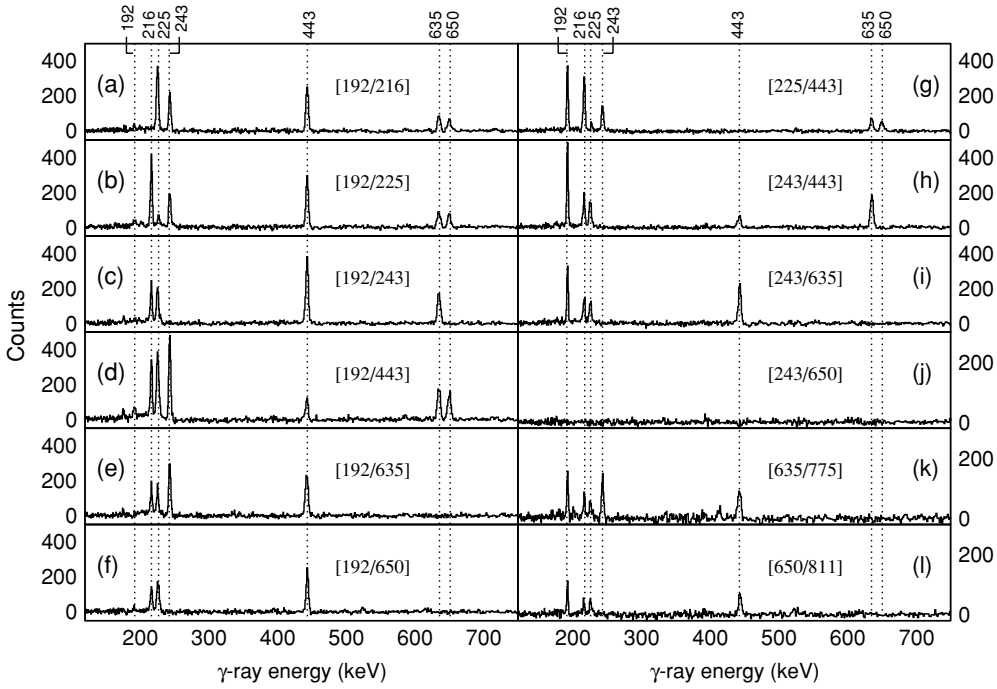

FIG. 3. Double-gated γ-ray coincidence spectra, projected from the particle-gated cube, showing some of the coincidence relationships used in the placement of the low-energy transitions. Double gates used to generate the spectra are given as $[a/b]$, where a and b are the gating transitions in keV. Vertical numbers above the top panels are the transition energies in the low-spin part of the ^{116}Cs level scheme.

in the next section. The intensities of transitions measured in such spectra, in comparison to statistical model predictions for the more intense reaction channels, suggest a production cross section for ^{116}Cs of about 100 μb.

IV. RESULTS

A. Level scheme of ^{116}Cs

Using γ-ray coincidence relationships, together with energy and intensity measurements, the level scheme shown in Fig. 4 was deduced. In order to help assign spins and parities to the excited states, γ-ray angular-distribution measurements were made. Two $\gamma\gamma$ matrices were constructed, which were incremented with γ-ray energies from any germanium detector on one axis, and with γ-ray energies from detectors at a particular value of θ on the other axis. To increase the number of counts, detectors at θ and $(180^\circ - \theta)$ were summed. These matrices were gated on the αp, α, or p evaporation channels to enhance the relative amount of ^{116}Cs present. By gating on the "any" germanium-detector axis, the intensities of γ rays at a particular θ could be measured. Using this method, γ-ray intensities at $\theta \simeq 90^\circ$ (28 detectors at $\theta = 79.2^\circ, 80.7^\circ, 90.0^\circ, 99.3^\circ$, and 100.8°) and $\theta \simeq 40^\circ$ (38 detectors at $\theta = 31.7^\circ, 37.4^\circ, 50.1^\circ, 129.9^\circ, 142.6^\circ$, and 148.3°) were measured, and the angular-intensity ratio R of these intensities was taken. After normalizing to the number of detectors used, R was found to be near 0.8 for a stretched-dipole transition and near 1.3 for a stretched-quadrupole transition. These values were calibrated using transitions with known multipolarity in the ^{118}Cs [12,24] and ^{118}Xe [25] nuclei. The properties of the γ-ray transitions assigned to ^{116}Cs are summarized in Table I.

The arrangement of excited states was complicated by the fact that several pairs of transitions have very similar energies at $\sim$226, $\sim$243, and $\sim$443 keV. The pair of transitions with energies 225.1 and 226 keV are self-coincident and were thus relatively easily placed in the level scheme. Furthermore, it was found that gating on the 634.8-keV or 811.0-keV transitions eliminated one pair of 226-keV transitions from the spectra, suggesting that the decay path of one $\sim$226-keV transition is parallel to the 634.8- and 811-keV transitions. Both pairs of transitions at $\sim$243 and $\sim$443 keV were *not* found to be self-coincident, and the placement of the $\sim$443-keV transitions in the level scheme was further complicated by the existence of a tentative third transition at 442 keV. In the study of signature inversion, the arrangement of the low-spin states in the bands is of critical importance. For that reason, the placement of the $\sim$243 and $\sim$443-keV transitions is discussed further below.

From the eight most intense coincident transition energies associated with the 243- and 443-keV transitions, it was possible to construct 28 "double gates" for the particle-gated cube. The coincidence relationships derived from all of the double-gated spectra supported the arrangement of excited states shown in Fig. 4. Twelve of the double-gated spectra are shown in Fig. 3. For the $\sim$443-keV pair, it was possible to isolate one of the transitions by gating on higher-lying transitions: for example, in Fig. 3, panel (k) shows both of the $\sim$443-keV transitions, whereas panel (l) shows only the 443.2-keV transition. This comparison is shown on an expanded scale in Fig. 5, where panel (a) shows the spectrum that is double-gated on the 635- and 775-keV transitions and panel (b) shows that which is double-gated on the 650- and 811-keV transitions. The $\sim$443-keV peak on panel (a)

TABLE I. Properties of γ-ray transitions assigned to ^{116}Cs. First and second columns give energies and intensities of the γ rays, respectively. γ-ray intensities are normalized to the most intense γ ray, at 191.8 keV. Third column gives angular-distribution ratios R. Fourth column lists initial and final assigned spins and parities. Fifth column shows presumed γ-ray multipolarity. Data for the pairs of transitions at 243 and 443 keV are measured from the composite peaks in the spectra. See the text for details, such as the definition of R.

E_γ (keV)	I_γ	R	$I_i^{\pi_i} \rightarrow I_f^{\pi_f}$	Mult.
176	5(1)	1.82(14)	$10^+ \rightarrow$	
189	8(1)		$17^+ \rightarrow 16^+$	$M1/E2$
191.8	100(5)	1.27(4)		
216.2	64(3)	1.19(4)	$10^+ \rightarrow 8^+$	
225.1	79(4)	1.59(6)	$8^+ \rightarrow$	$E2$
226	10(2)	0.72(8)	$15^+ \rightarrow 14^+$	$M1/E2$
243	32(4)	0.77(2)	$11^+ \rightarrow 10^+$	$M1/E2$
243	32(4)	0.77(2)	$13^+ \rightarrow 12^+$	$M1/E2$
442	10(3)		$10^+ \rightarrow$	
443.2	56(6)	1.42(5)	$12^+ \rightarrow 10^+$	$E2$
442.8	56(6)	1.42(5)	$13^+ \rightarrow 11^+$	$E2$
634.8	24(2)	1.37(5)	$15^+ \rightarrow 13^+$	$E2$
650.0	20(2)	1.24(5)	$14^+ \rightarrow 12^+$	$E2$
774.5	21(2)	1.40(5)	$17^+ \rightarrow 15^+$	$E2$
811.0	11(1)	1.60(7)	$16^+ \rightarrow 14^+$	$E2$
873.1	21(2)	1.45(6)	$19^+ \rightarrow 17^+$	$E2$
925.5	9(1)	1.31(6)	$18^+ \rightarrow 16^+$	$E2$
942.3	20(2)	1.30(5)	$21^+ \rightarrow 19^+$	$E2$
983.7	6(1)		$24^+ \rightarrow 22^+$	$E2$
986.7	13(1)	1.33(6)	$23^+ \rightarrow 21^+$	$E2$
998.5	10(3)	1.46(8)	$22^+ \rightarrow 20^+$	$E2$
1018.7	10(3)	1.65(10)	$20^+ \rightarrow 18^+$	$E2$
1053.8	8(3)		$25^+ \rightarrow 23^+$	$E2$
1069.4	2(1)		$26^+ \rightarrow 24^+$	$E2$
1167.8	5(2)		$27^+ \rightarrow 25^+$	$E2$
1264.7	3(1)		$29^+ \rightarrow 27^+$	$E2$
1365.1	3(1)		$31^+ \rightarrow 29^+$	$E2$

has a lower centroid and a larger full-width-at-half-maximum (FWHM) than that shown on panel (b). Use of such spectra enabled energies of 442.8 and 443.2 keV to be assigned to the two ∼443-keV transitions. However, the method by which these energies were assigned leads to a large associated uncertainty, estimated to be around 0.4 keV. Given the level scheme shown in Fig. 4, an energy difference between the ∼443-keV transitions would require a corresponding energy difference in the ∼243-keV transitions. It was not possible to isolate either of the ∼243-keV transitions by judicious gating, and thus it was not possible to accurately measure the energy of either transition. The energy of each transition is therefore given as 243 keV.

The spectrum shown in Fig. 3, panel (d) is double-gated on the 192- and ∼443-keV transitions, and that in panel (h) is double-gated on the 243- and ∼443-keV transitions; both spectra show evidence for the tentative third transition, at 442 keV. The 442-keV transition is clearly not present on panel (g), which is gated on the 443- and the 225-keV transitions,

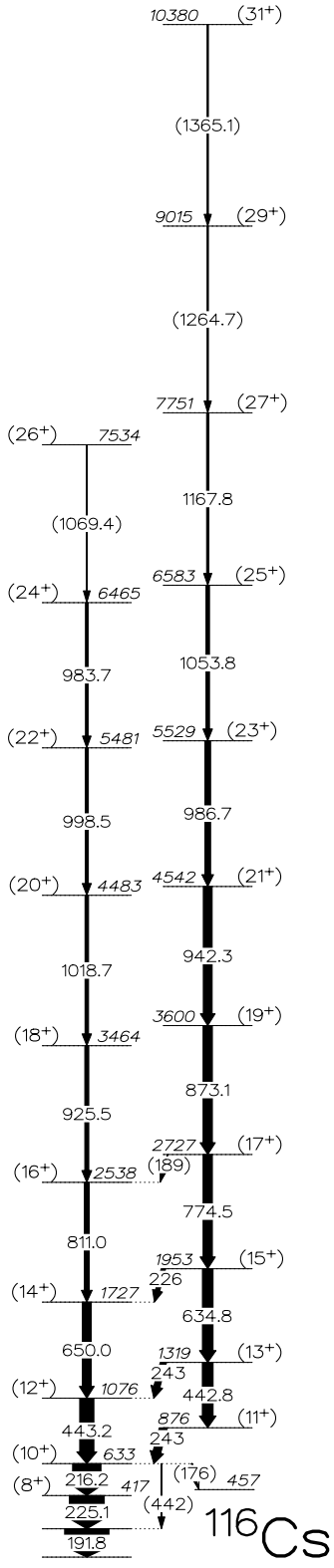

FIG. 4. Level scheme of the $\nu(h_{11/2}) \otimes \pi(h_{11/2})$ band in ^{116}Cs deduced in this work. Excitation energies are given relative to the lowest state shown. Spins and parities are assigned from systematics and are thus tentative. Transitions with energies in parentheses are tentatively placed. Uncertainties in the energies are 0.1 to 0.4 keV; uncertainties in the intensities are $\leqslant$10%.

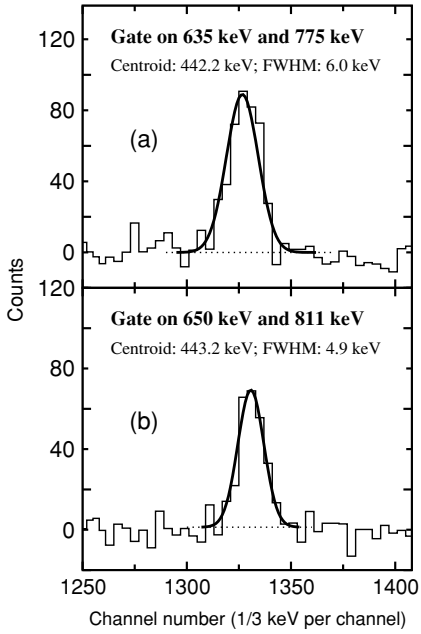

FIG. 5. Comparison of 443-keV peaks in two double-gated spectra. The peak in (a) has a lower centroid and a larger FWHM than that in (b), suggesting that (a) shows a composite peak, whereas (b) shows a peak corresponding to a single transition. A Gaussian fit to each peak (bold line) and the associated background (dotted line) are also shown.

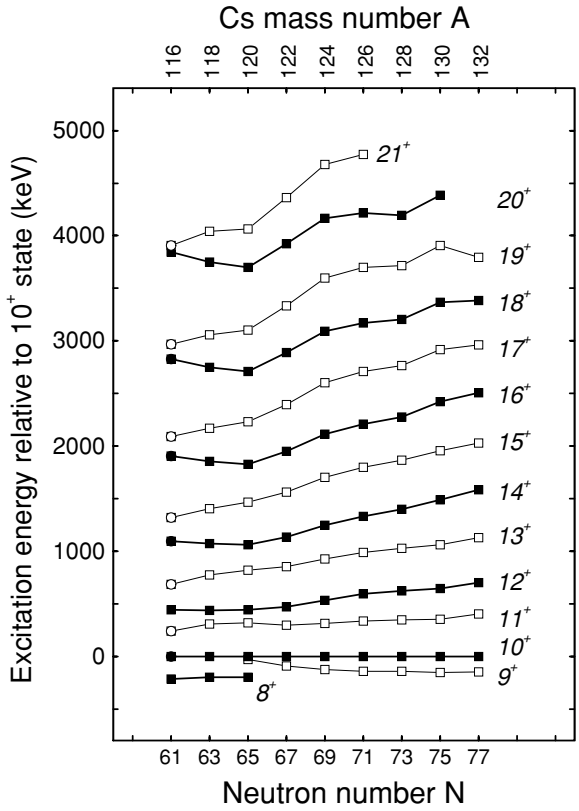

FIG. 6. Excitation-energy systematics of states with $I \leqslant 21\hbar$ in the $\nu(h_{11/2}) \otimes \pi(h_{11/2})$ bands of the odd-odd cesium isotopes with $116 \leqslant A \leqslant 132$. Data for $^{118-128}$Cs are taken from Refs. [8,11,12,14, 16,30]; data for ^{116}Cs are from this work. Excitation energies are given relative to the respective 10^+ states in each band.

demonstrating that the 442-keV transition decays in parallel to the 225-keV transition.

The parallel paths of two 243- and 443-keV transitions made meaningful intensity measurements very difficult. For example, because it was not possible to isolate either transition in the 243-keV pair, it was not possible to accurately determine the intensity of either transition. Although it was possible to isolate either ∼443-keV transition by gating on higher-lying transitions, the intensities were then biased by the gating transitions and had significant associated uncertainties. The placement of the ∼243 and ∼443-keV transitions in Fig. 4 is therefore largely based on coincidence relationships and the properties of the composite peaks in the spectra.

B. Spin assignments

The yrast bands of the neighboring heavier cesium isotopes are based upon the $\nu(h_{11/2}) \otimes \pi(h_{11/2})$ configuration. Over the range $118 \leqslant A \leqslant 132$, the spins of these bands have been unambiguously measured in five cases: ^{120}Cs [13]; ^{122}Cs [15]; ^{124}Cs [16]; ^{130}Cs [26]; and ^{132}Cs [27]. Systematic spin assignments have also been made for these isotopes in Refs. [28,29]. The systematic studies make use of the fact that the $\nu(h_{11/2}) \otimes \pi(h_{11/2})$ configurations are known to be well deformed and, as a result, the excitation energies of states within the bands vary smoothly as a function of neutron number; this trend is observed in the $\pi(h_{11/2})$ bands of the odd-A $^{117-133}$Cs isotopes, and in the ground-state bands of the even-even $Z = 54$ $^{116-130}$Xe isotopes. In Ref. [29], a study of the excitation energies, together with alignment-additivity arguments, has arrived at a consistent set of spin assignments. In Ref. [28], spin assignments are proposed based upon the assumption that the moments of inertia should smoothly decrease with increasing neutron number. These systematic spin assignments are consistent with each other and with the spins measured in Refs. [16,26,27].

As discussed later, the $\nu(h_{11/2}) \otimes \pi(h_{11/2})$ configuration in ^{116}Cs is expected to be well deformed, and thus the band in ^{116}Cs should continue the smooth trend in excitation energies. The excitation-energy systematics for the $\nu(h_{11/2}) \otimes \pi(h_{11/2})$ bands in the odd-odd cesium isotopes with $116 \leqslant A \leqslant 132$ are shown in Fig. 6, where the energies are given relative to the assigned 10^+ state for each isotope. The spins in the figure are taken from the systematic studies of Refs. [28,29], which are thus also in agreement with the measurements of Refs. [16,26,27]. Clearly, a smooth trend is observed, which continues for ^{116}Cs, given the spin assignments on the level scheme. The measurements by Moon *et al*. [13,15] suggest that the spins for ^{120,122}Cs are $2\hbar$ higher than those given in Fig. 6. Unless there is a discontinuity in the excitation energy systematics, it would appear that the measurements of Moon *et al*. are not consistent with those of Refs. [16,26,27].

In the present work, the spin assignments given in Figs. 4 and 6 have been adopted for the ^{116}Cs band. It should be remembered, however, that these assignments are tentative, and that it is possible that the spins of all of the isotopes shown are $2\hbar$ higher, in accordance with the measurements of

Moon *et al*. The approach used here cannot distinguish whether the bandhead is the assigned 8^+ or 10^+ state—both follow the smooth trend. The yrast states of neighboring $^{115}_{54}Xe_{61}$ [31] and $^{117}_{55}Cs_{62}$ [32] form decoupled bands based upon $\nu(h_{11/2})$ and $\pi(h_{11/2})$ orbitals, respectively, both with bandhead spins of 11/2. The bandhead for ^{116}Cs has been assigned to be the 10^+ state, which is the sum of the decoupled neutron and proton spins in parallel. With that assumption, in the band assigned to ^{116}Cs, the even-spin sequence then consists of eight $E2$ transitions extending from the (10^+) state at 633 keV to the (26^+) state at 7534 keV: and the odd-spin sequence consists of ten $E2$ transitions extending from the (11^+) state at 876 keV to the (31^+) state at 10 380 keV. The odd-spin states decay into the even-spin states via three (tentatively four) $\Delta I = 1$, mixed $M1/E2$ transitions over the spin range (11) to (17)$\hbar$.

Below the (10^+) state are three intense transitions, with energies 192, 216, and 225 keV. The measured angular-distribution ratios of these transitions are consistent with the $E2$ character. The existence of the 442-keV transition, albeit tentative, suggests that the 225-keV transition may be of nonstretched, mixed $M1/E2$ character. A tentative 176-keV transition has been assigned to decay from the (10^+) state. Because the origin of the states below the (10^+) state is not clear, tentative spin assignments are not proposed. Previous work [33] has revealed that two states in ^{116}Cs decay by both β-delayed proton and α-particle emission, with half-lives of $\sim$0.7 and $\sim$3.5 s, and with tentatively assigned spins of 1 and >4, respectively. However, it was not established which of the states is the ground state. In the present work, because it was not possible to determine the spin of the lowest state observed, it is not known whether this level correspnds to the ground state or a low-lying isomeric state. The excitation energies in Fig. 4 are, therefore, relative to the lowest lying state shown, not to the ground state.

V. DISCUSSION

A. Quasiparticle alignments

A study of the aligned angular momentum has been used to further investigate the configuration assignment. The expected quasiparticle alignment frequencies have been obtained with cranked shell-model (CSM) calculations [34], assuming deformation parameters from total-Routhian surface (TRS) calculations [28,35,36] as discussed in the next section. The CSM predicts that for ^{116}Cs, the first pairs of $h_{11/2}$ neutrons (EF, in the usual nomenclature) and $h_{11/2}$ protons (ef) will align at rotational frequencies $\sim$0.34 and $\sim$0.38 MeV/$\hbar$, respectively. The second $h_{11/2}$ neutron pair (FG) is predicted to align at $\sim$0.45 MeV/$\hbar$, while the second $h_{11/2}$ proton pair (fg) is not predicted to align until $\sim$0.60 MeV/$\hbar$. If the band is based on the $\nu(h_{11/2}) \otimes \pi(h_{11/2})$ configuration, the first $h_{11/2}$ neutron and proton alignments (EF and ef) will be blocked, but alignments of the second pairs (FG and fg) should be observed. The aligned angular momentum of the even spin ($\alpha = 0$) sequence in ^{116}Cs is shown in Fig. 7 in comparison with the analogous sequences in the $\nu(h_{11/2}) \otimes \pi(h_{11/2})$ bands of ^{118,120}Cs. The calculated frequencies of alignment of the ef, EF, fg, and FG pairs in ^{116}Cs are indicated on the figure by vertical dotted lines. All of the bands have very similar initial values of aligned angular momentum, and they start to bend upward around 0.5 MeV/$\hbar$. The upbend is more pronounced in ^{116}Cs owing to a weaker interaction strength. In ^{116}Cs, the upbend is observed at about 0.47 MeV/$\hbar$, which is consistent with the frequency of the predicted alignment of the second pair of neutrons (FG), and which in turn is consistent with the proposed $\nu(h_{11/2}) \otimes \pi(h_{11/2})$ assignment.

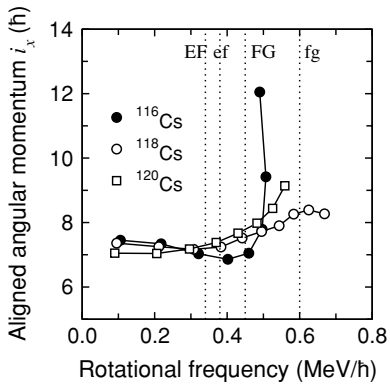

FIG. 7. Aligned angular momenta in the $\nu(h_{11/2}) \otimes \pi(h_{11/2})$ even-spin ($\alpha = 0$) bands in ^{116,118,120}Cs. Data are from Refs. [11,12], except for ^{116}Cs, data from this work. For all data points, a reference configuration with the Harris parameters [37] $\mathcal{J}_0 = 17.0$ MeV$^{-1}\hbar^2$ and $\mathcal{J}_1 = 25.8$ MeV$^{-3}\hbar^4$ [38] has been subtracted. Values of $K = 3, 4, 5$ have been assumed for ^{116,118,120}Cs, respectively. The vertical dotted lines mark the rotational frequencies at which the ef, EF, fg, and FG alignments are predicted by the CSM for ^{116}Cs, as discussed in the text.

B. Signature inversion and extended TRS calculations

Since the first observation of signature inversion (references within Ref. [1]), numerous theoretical explanations have been put forward. Initially, the phenomenon was attributed to triaxiality of the nuclear shape (with $\gamma > 0^\circ$ in the Lund convention) along with specific positions of the Fermi levels [1]. Later, signature inversion was observed in axially symmetric nuclei [11] and interpretations without triaxial deformation were presented. Calculations involving a residual np interaction within the framework of the particle-rotor model [39,40] have reproduced observed signature inversions [11]. In a completely different approach, signature inversions have been reproduced with axially symmetric shapes using the projected shell model, where signature inversion arises due to a band crossing [41].

Some of the most recent theoretical work has found that a quadrupole-pairing interaction can give rise to signature inversion. The origins of the effect are discussed in Ref. [28]. In essence, the effect is due to K mixing caused by the mean-field contribution of the quadrupole-pairing interaction (specifically the Q_{22} component [28]). The effect can be viewed as an enhancement of deformation-induced signature inversion (for example, due to triaxiality) with the size of the overall effect depending on the positions of the Fermi levels and on the deformation. Extended TRS calculations performed in Ref. [28] reproduce the observed signature inversions for odd-odd $^{120-124}$Cs and for several odd-odd $A = 160$ isotopes.

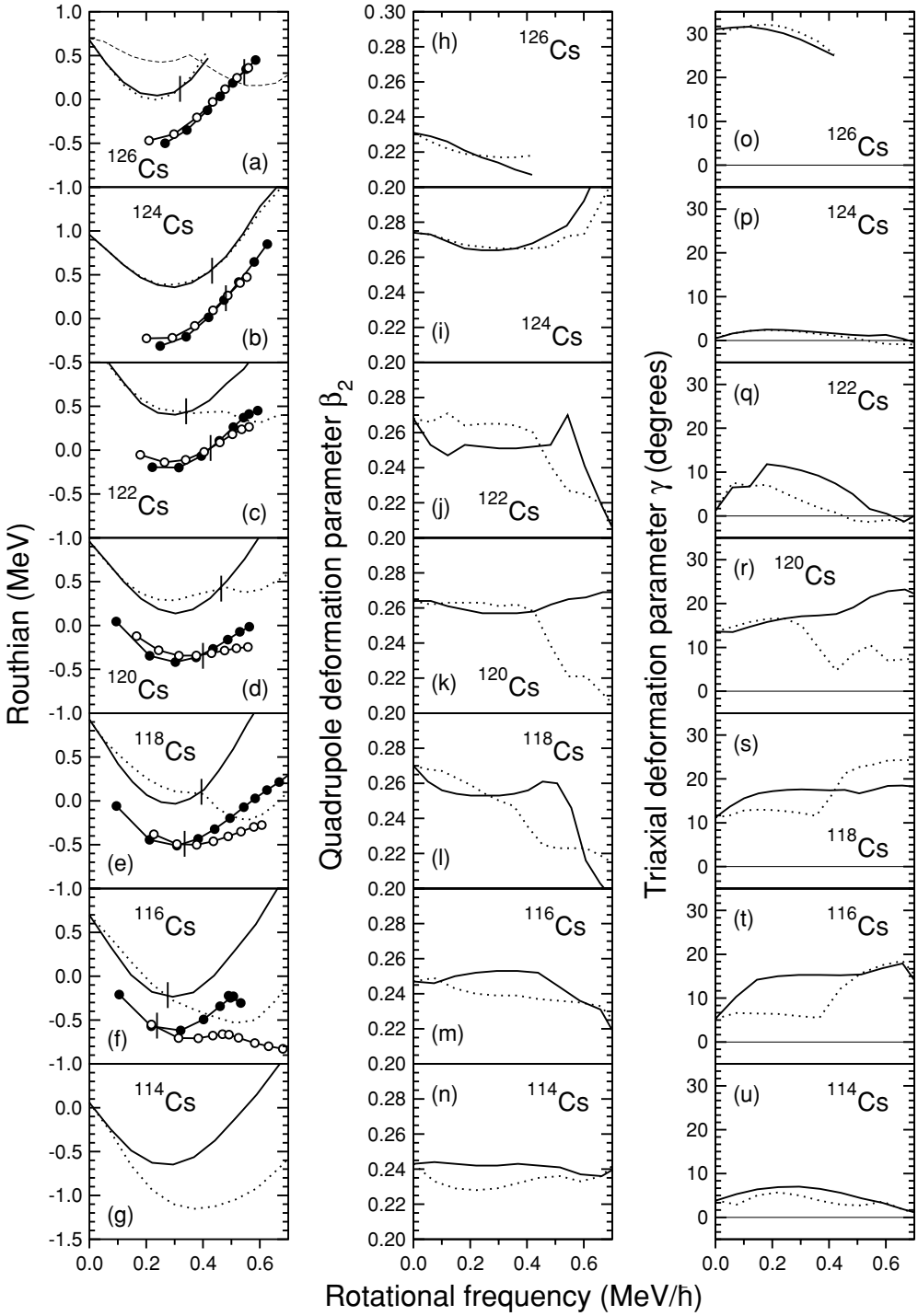

FIG. 8. Extended TRS calculation results for $\nu(h_{11/2}) \otimes \pi(h_{11/2})$ configurations in odd-odd $^{114-126}$Cs isotopes. Panels (a) to (g) show Routhians; (h) to (n), quadrupole deformation parameters β_2; (o) to (u), triaxial deformation parameters γ. For all calculated data, solid lines represent the *expected* unfavored signature ($\alpha = 0$); dotted lines, the *expected* favored signature ($\alpha = 1$). Also, (a) to (f) give the experimentally extracted Routhians: favored signature states (open circles) and unfavored signature states (filled circles). In (a) to (f), the rotational frequencies at which the Routhians cross is marked by a short vertical line, and a reference Routhian with Harris parameters $\mathcal{J}_0 = 44.0$ MeV$^{-1}\hbar^2$ and $\mathcal{J}_1 = 0.0$ MeV$^{-3}\hbar^4$ has been subtracted [28]. For ease of comparison between calculations and experimental data, some of the experimental Routhians have been given an energy offset: ^{118,120,122}Cs, $+0.5$ MeV; ^{126}Cs, -0.5 MeV. Dashed line in (a) represents the minimum with $\gamma = -30°$, which becomes lowest in energy above 0.4 MeV/$\hbar$, as discussed in the text.

In order to investigate signature inversion in ^{116}Cs and the neighboring cesium isotopes, extended TRS calculations have been carried out systematically for $\nu(h_{11/2}) \otimes \pi(h_{11/2})$ configurations in the isotopes $^{114-126}$Cs. The model is based on the traditional TRS approach, described in Refs. [35,36], but is *extended* by the inclusion of quadrupole-pairing correlations, particle-number projection, and a proper treatment of blocking. The model and its dependence on parameters were fully described in Ref. [28]. Some results of the calculations are presented in Fig. 8: panels (a) to (g) give Routhians, (h) to (n) give quadrupole deformation parameters β_2, and (o) to (u) show the triaxial deformation parameters γ. The experimental Routhians are also given in (a) to (f). For both calculated and experimental data, a reference Routhian with Harris parameters [37] $\mathcal{J}_0 = 44.0$ MeV$^{-1}\hbar^2$ and $\mathcal{J}_1 = 0.0$ MeV$^{-3}\hbar^4$ has been subtracted, as in Ref. [28]. The absolute excitation energies of some of the observed bands are not known; the figure, therefore, only compares the *relative* differences between the Routhians, and for ease of comparison, an energy offset has been added to some of the experimental Routhians, as indicated in the figure caption. On panels (a) to (f), the signature-inversion frequencies are marked by short vertical lines. Bands based on the $\nu(h_{11/2}) \otimes \pi(h_{11/2})$ configuration have favored signature $\alpha_f = 1$ and unfavored signature $\alpha_u = 0$: the states with odd spins ($\alpha = 1$) should lie lower in energy than those with even spins ($\alpha = 0$).

Inspection of Fig. 8(f) reveals that ^{116}Cs exhibits signature inversion at a rotational frequency of $\sim$0.23 MeV/$\hbar$. Thus, the present results extend the observation of signature inversion in the cesium isotopes to $A = 116$ ($N = 61$). For ^{116}Cs, the calculated signature inversion frequency is 0.26 MeV/$\hbar$, which is close to that observed. Below a rotational frequency of 0.4 MeV/$\hbar$, the agreement between the relative trajectories of the experimental and calculated Routhians is reasonably good. Generally, for all of the isotopes $^{116-124}$Cs, the experimental Routhians are reasonably well reproduced. For ^{120,118,116}Cs, the calculated inversion frequencies decrease with decreasing N; they are slightly larger than those observed, but the differences are less than 100 keV/$\hbar$. For ^{124,122}Cs, the signature splitting before the inversion and the inversion frequencies are reproduced, but the observed trend of decreasing frequency with decreasing N is not continued. The observed behavior in ^{126}Cs does not agree at all with the calculated value.

The isotopes ^{120,118,116}Cs have triaxial deformation parameters of $\gamma = 15$–20°, whereas the γ values for ^{124,122}Cs are smaller with $\gamma < 10^\circ$ for ^{122}Cs, and $\gamma = 3^\circ$ for ^{124}Cs. As reported in Ref. [28], the signature splitting is dominated by triaxiality. The signature inversions in ^{120,118,116}Cs are therefore largely due to the effects of their sizable triaxial deformations, with the effects of quadrupole-pairing correlations playing a less significant role. For the nucleus ^{124}Cs, the converse is true with the quadrupole-pairing effect significantly enhancing the observed inversion. The isotope ^{122}Cs is an intermediate case between ^{120,118,116}Cs and ^{124}Cs.

For ^{126}Cs, a different behavior is observed. This isotope has a more pronounced triaxiality with $\gamma = 30^\circ$. Also, for the favored signature of the $\nu(h_{11/2}) \otimes \pi(h_{11/2})$ configuration in ^{126}Cs, a minimum with $\gamma = -30^\circ$ is lower in energy above a rotational frequency of 0.4 MeV/$\hbar$ (spin of 16 or 17$\hbar$); the Routhians associated with this minimum are shown by the dashed line on Fig. 8(a). For ^{126}Cs, the wave functions of states in these coexisting minima will mix, in particular because the shape of the nucleus is soft with respect to nonaxial deformations. Therefore, for ^{126}Cs, configuration mixing and dynamics will be important factors governing the signature splitting. Such effects are not included in the mean-field approach used in the extended TRS calculations. As a result, this approach does not reliably reproduce the behavior of the ^{126}Cs Routhians.

For the $N = 59$ isotope, ^{114}Cs, the calculated Routhians do not undergo signature inversion: the favored signature always lies lower in energy [Fig. 8(g)]. The absence of signature inversion is presumed to be due to large Coriolis-induced signature splitting caused by the proximity of the neutron Fermi level to the $\Omega = 1/2\ h_{11/2}$ orbital, in conjunction with a reasonably small triaxial deformation of $\gamma = 6^\circ$. This Coriolis-induced signature splitting at $N = 59$ will dominate over the anomalous signature splitting induced by quadrupole-pairing correlations. This can be contrasted with the $N = 61$ odd-odd neighbor, ^{116}Cs, where the Coriolis-induced signature splitting is smaller due to the neutron Fermi level lying higher in the $h_{11/2}$ subshell, and the triaxiality is larger with $\gamma \simeq 16^\circ$. For ^{116}Cs, both of these effects, in addition to the effects of quadrupole-pairing correlations, combine to produce signature inversion.

VI. SUMMARY

In summary, excited states have been observed for the first time in the very neutron-deficient ^{116}Cs nucleus. A rotational band presumed to be based on the $\nu(h_{11/2}) \otimes \pi(h_{11/2})$ configuration has been assigned to ^{116}Cs by detecting γ rays in coincidence with evaporated charged particles and with evaporation residues. Tentative spins have been assigned to the band by extrapolating from measured spins in bands based on the same configuration in neighboring nuclei, assuming systematic behavior as a function of N. The band exhibits signature inversion at a rotational frequency of 0.23 MeV/$\hbar$, which corresponds to assigned spins of 12–13 $\hbar$. The signature inversions in the odd-odd cesium isotopes have been compared to the results of extended TRS calculations, in which the underlying mechanism responsible for signature inversion is a combination of a triaxial nuclear shape and quadrupole-pairing correlations. The calculations reproduce the data for $^{116-124}$Cs reasonably well and predict that ^{116}Cs is the lightest cesium isotope in which signature inversion will occur. The study of the very neutron-deficient cesium isotopes presents an excellent test of various mean-field models (such as Skyrme Hartree-Fock calculations, relativistic mean-field calculations, and calculations with the Gogny force). It would be interesting to determine which of the calculations can account for the observed signature splittings.

ACKNOWLEDGMENTS

This work was supported by the EPSRC, and by the U.S. Department of Energy, Office of Nuclear Physics, under Contract Nos. W-31-109-ENG-38 (ANL) and DE-FG02-88ER-40406 (Washington University).

[1] R. Bengtsson, H. Frisk, F. R. May, and J. A. Pinston, Nucl. Phys. **A415**, 189 (1984).

[2] Y. Liu, Y. Ma, H. Yang, and S. Zhou, Phys. Rev. C **52**, 2514 (1995).

[3] Y. Liu, J. Lu, Y. Ma, S. Zhou, and H. Zheng, Phys. Rev. C **54**, 719 (1996).

[4] L. L. Riedinger, D. J. Hartley, A. Galindo-Uribarri, B. H. Smith, C. Baktash, M. P. Carpenter, M. Danchev, M. Devlin, C. J. Gross, R. V. F. Janssens, M. Lipoglavsek, S. D. Paul, D. C. Radford, W. Reviol, D. G. Sarantites, D. Seweryniak, C.-H. Yu, and O. Zeidan, Acta Phys. Pol. B **32**, 2613 (2001).

[5] Aage Bohr and Ben R. Mottelson, *Nuclear Structure, Vol. II: Nuclear Deformations* (World Scientific, Singapore, 1998).

[6] Ikuko Hamamoto, Phys. Lett. **B235**, 221 (1990).

[7] R. Bengtsson and S. Frauendorf, Nucl. Phys. **A327**, 139 (1979).

[8] T. Komatsubara, K. Furuno, T. Hosoda, J. Mukai, T. Hayakawa, T. Morikawa, Y. Iwata, N. Kato, J. Espino, J. Gascon, N. Gjorup, G. B. Hagemann, H. J. Jensen, D. Jerrestam, J. Nyberg, G. Sletten, B. Cederwall, and P. O. Tjom, Nucl. Phys. **A557**, 419c (1993).

[9] R. Zheng, S. Zhu, N. Cheng, and J. Wen, Phys. Rev. C **64**, 014313 (2001).

[10] C. Plettner, I. Ragnarsson, H. Schnare, R. Schwengner, L. Kaubler, F. Dönau, A. Algora, G. de Angelis, D. R. Napoli, A. Gadea, J. Eberth, T. Steinhardt, O. Thelen, M. Hausmann, A. Müller, A. Jungclaus, K. P. Lieb, D. G. Jenkins, R. Wadsworth, and A. N. Wilson, Phys. Rev. Lett. **85**, 2454 (2000).

[11] B. Cederwall, F. Liden, A. Johnson, L. Hildingsson, R. Wyss, B. Fant, S. Juutinen, P. Ahonen, S. Mitarai, J. Mukai, J. Nyberg, I. Ragnarsson, and P. B. Semmes, Nucl. Phys. **A542**, 454 (1992).

[12] J. F. Smith, C. J. Chiara, D. B. Fossan, G. R. Gluckman, G. J. Lane, J. M. Sears, I. Thorslund, H. Amro, C. N. Davids, R. V. F. Janssens, D. Seweryniak, I. M. Hibbert, R. Wadsworth, I. Y. Lee, and A. O. Macchiavelli, Phys. Lett. **B406**, 7 (1997).

[13] C.-B. Moon, S. J. Chae, J. H. Ha, T. Komatsubara, Y. Sasaki, T. Jumatsu, K. Yamada, K. Satou, and K. Furuno, Nucl. Phys. **A696**, 45 (2001).

[14] J. F. Smith, C. J. Chiara, D. B. Fossan, G. J. Lane, J. F. Lewicki, J. M. Sears, and P. Vaska, Phys. Rev. C **58**, 3237 (1998).

[15] C.-B. Moon, T. Komatsubara, and K. Furuno, Nucl. Phys. **A674**, 343 (2000).

[16] J. Lu, Y. Liu, L. Yin, G. Zhao, F. Zhang, X. Li, R. Meng, Z. Wang, Y. Ma, Z. Wang, J. Huo, X. Wu, S. Wen, G. Li, and C. Yang, Phys. Rev. C **62**, 057304 (2000).

[17] A. Gizon, J. Timár, J. Gizon, B. Weiss, D. Barnéoud, C. Foin, J. Genevey, F. Hannachi, C. F. Liang, A. Lopez-Martens, P. Paris, B. M. Nyakó, L. Zolnai, J. C. Merdinger, S. Brant, and V. Paar, Nucl. Phys. **A694**, 63 (2001).

[18] X.-F. Li, Y.-J. Ma, Y.-Z. Liu, J.-B. Lu, G.-Y. Zhao, L.-C. Yin, R. Meng, Z.-L. Zhang, L.-J. Wen, X.-H. Zhou, Y.-X. Guo, X.-G. Lei, Z. Liu, Y. Zheng, and J.-J. He, Eur. Phys. J. A **17**, 523 (2003).

[19] P. J. Nolan, F. A. Beck, and D. B. Fossan, Annu. Rev. Nucl. Part. Sci. **44**, 561 (1994).

[20] D. G. Sarantites, P.-F. Hua, M. Devlin, L. G. Sobotka, J. Elson, J. T. Hood, D. R. LaFosse, J. E. Sarantites, and M. R. Maier, Nucl. Instrum. Methods Phys. Res. A **381**, 418 (1996).

[21] C. N. Davids, B. B. Back, K. Bindra, D. J. Henderson, W. Kutschera, T. Lauritsen, Y. Nagame, P. Sugathan, A. V. Ramayya, and W. B. Walters, Nucl. Instrum. Methods Phys. Res. B **70**, 358 (1992).

[22] D. C. Radford, Nucl. Instrum. Methods Phys. Res. A **361**, 297 (1995).

[23] F. Plasil and M. Blann, Phys. Rev. C **11**, 508 (1975).

[24] A. B. Kamdar, M.Sc. thesis, University of Manchester, 2003.

[25] J. M. Sears, D. B. Fossan, G. R. Gluckman, J. F. Smith, I. Thorslund, E. S. Paul, I. M. Hibbert, and R. Wadsworth, Phys. Rev. C **57**, 2991 (1998).

[26] P. R. Sala, N. Blasi, G. Lo Bianco, A. Mazzoleni, R. Reinhardt, K. Schiffer, K. P. Schmittgen, G. Siems, and P. Von Brentano, Nucl. Phys. **A531**, 383 (1991).

[27] G. Rainovski, E. S. Paul, H. J. Chantler, P. J. Nolan, D. G. Jenkins, R. Wadsworth, P. Raddon, A. Simons, D. B. Fossan, T. Koike, K. Starosta, C. Vaman, E. Farnea, A. Gadea, Th. Kroll, G. de Angelis, R. Isocrate, D. Curien, and V. I. Dimitrov, J. Phys. G **29**, 2763 (2003).

[28] F. R. Xu, W. Satuła, and R. Wyss, Nucl. Phys. **A669**, 119 (2000).

[29] Y. Liu, J. Lu, Y. Ma, G. Zhao, H. Zheng, and S. Zhou, Phys. Rev. C **58**, 1849 (1998).

[30] T. Koike, K. Starosta, C. J. Chiara, D. B. Fossan, and D. R. LaFosse, Phys. Rev. C **67**, 044319 (2003).

[31] E. S. Paul, A. J. Boston, S. Courtin, P. J. Dagnall, J. L. Durell, C. Finck, B. Gall, B. Haas, F. Haas, F. Hannachi, F. Hoellinger, J. C. Lisle, A. Lopez-Martens, J. C. Merdinger, N. Rowley, H. C. Scraggs, O. Stezowski, B. J. Varley, and J. P. Vivien, Eur. Phys. J. A **7**, 449 (2000).

[32] J. F. Smith, V. Medina-Chico, C. J. Chiara, D. B. Fossan, G. J. Lane, J. M. Sears, I. Thorslund, H. Amro, C. N. Davids, R. V. F. Janssens, D. Seweryniak, I. M. Hibbert, R. Wadsworth, I. Y. Lee, and A. O. Macchiavelli, Phys. Rev. C **63**, 024319 (2001).

[33] P. Tidemand-Petersson, R. Kirchner, O. Klepper, E. Roeckl, D. Schardt, A. Plochocki, and J. Zylicz, Nucl. Phys. **A437**, 342 (1985).

[34] W. Nazarewicz, J. Dudek, R. Bengtsson, T. Bengtsson, and I. Ragnarsson, Nucl. Phys. **A435**, 397 (1985).

[35] R. Wyss, J. Nyberg, A. Johnson, R. Bengtsson, and W. Nazarewicz, Phys. Lett. **B215**, 211 (1988).

[36] W. Nazarewicz, R. Wyss, and A. Johnson, Nucl. Phys. **A503**, 285 (1989).

[37] Samuel Harris, Phys. Rev. **138**, B509 (1965).

[38] D. M. Todd *et al*., J. Phys. G **10**, 1407 (1984).

[39] N. Tajima, Nucl. Phys. **A572**, 365 (1994).

[40] P. B. Semmes and I. Ragnarsson, in *Conference on High-Spin Physics and Gamma Soft Nuclei*, edited by J. X. Saladin, R. A. Sorenson, and C. M. Vincent (World Scientific, Singapore, 1991), p. 500.

[41] K. Hara and Y. Sun, Nucl. Phys. **A531**, 221 (1991).